

The uniaxial strain test - a simple method for the characterization of porous materials

T. Fiedler[†]

Centre for Mechanical Technology and Automation, University of Aveiro, Aveiro, Portugal

A. Öchsner[‡] and J. Grácio[‡]

Centre for Mechanical Technology and Automation, University of Aveiro, Aveiro, Portugal
Department of Mechanical Engineering, University of Aveiro, Aveiro, Portugal

(Received February 25, 2005, Accepted October 17, 2005)

Abstract. The application of cellular materials in load-carrying and security-relevant structures requires the exact prediction of their mechanical behavior, which necessitates the development of robust simulation models and techniques based on appropriate experimental procedures. The determination of the yield surface requires experiments under multi-axial stress states because the yield behavior is sensitive to the hydrostatic stress and simple uniaxial tests aim only to determine one single point of the yield surface. Therefore, an experimental technique based on a uniaxial strain test for the description of the influence of the hydrostatic stress on the yield condition in the elastic-plastic transition zone at small strains is proposed and numerically investigated. Furthermore, this experimental technique enables the determination of a second elastic constant, e.g., Poisson's ratio.

Key words: multi-axial testing; cellular solids; plasticity; yield surface; nonlinear behavior.

1. Introduction

Cellular metals, e.g., metal foams (cf. Fig. 1), exhibit unique mechanical and physical properties that differ strongly from classical solid materials and are currently being considered for use in lightweight structures such as cores of sandwich panels or as passive safety components of automobiles, (Gibson and Ashby 1997). Interesting combinations of their mechanical and physical properties, such as relatively high stiffness in conjunction with very low weight or high gas permeability combined with high thermal conductivity, offer the possibility for new future-oriented multifunctional applications, e.g., in aviation and space technology.

The mechanical properties of cellular metals, in particular their resistance to plastic deformation, the evolution and progress of damage and fracture within the material, are determined by the microstructure and the cell wall material, respectively. The most important structural parameters which characterise a cellular metal are the morphology of the cell (geometry, open or closed cell),

[†] PhD Student, Corresponding author, E-mail: tfiedler@mec.ua.pt

[‡] Professor

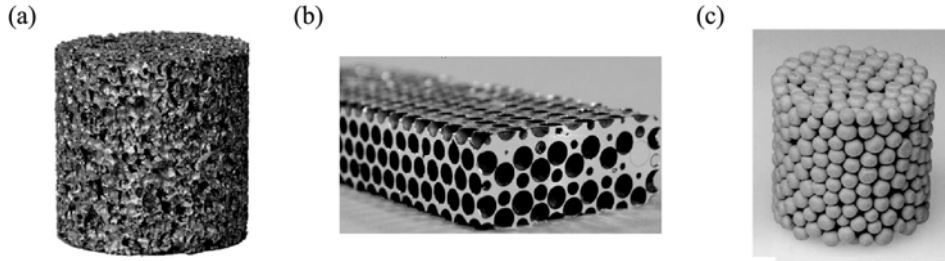


Fig. 1 Different types of cellular materials: (a) Closed-cell metal foam (ALPORAS[®]), (b) Hollow alumina spheres embedded in a magnesium matrix, (Körner and Singer 2000), (c) Hollow sphere foam Fe_{0.88}Cr_{0.12}, (Körner and Singer 2000)

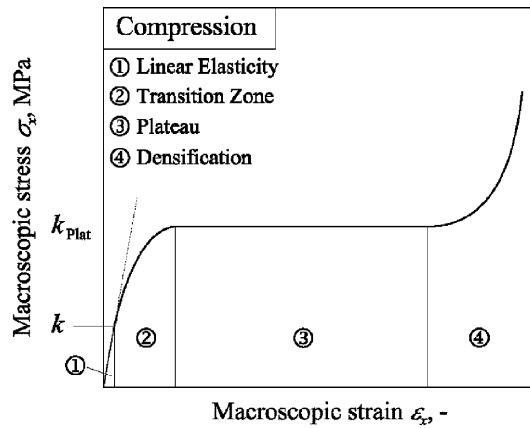


Fig. 2 Schematic uniaxial stress-strain curve for a metal foam in compression

the topology, the mean cell size and the relative density ρ/ρ_{solid} (the macroscopic density ρ divided by that of the solid material of the cell wall ρ_{solid} , (Ashby *et al.* 2000). However, there are still technological problems related to the control of the structure and properties of the cellular material, which remain to be solved. The vast majority of existing techniques do not allow for precise control of shape, size and distribution of the pores. That brings about a wide scatter in mechanical and other characteristics of the materials and components.

A schematic uniaxial compression stress-strain curve for cellular metal is shown in Fig. 2. It shows linear elasticity at low stress, followed by an elastic-plastic transition zone, which is followed by a long collapse plateau, truncated by a regime of densification in which the stress rises exponentially. Each of these four regions requires its own constitutive equation since the deformation mechanisms are quite different. Many investigations focus on the large deformations taking place in zones 3 and 4 where the inelastic behavior is governed by buckling, collapsing, and crushing of cells (Kiser *et al.* 1999, Hartmann *et al.* 1998, Balch and Dunand 2002, Gong and Kyriakides 2005). The initial yield stress k is equated in many analytical models with the plateau stress k_{plat} , so that the transition zone, which can be clearly distinguished in certain cellular materials, remains unconsidered (e.g., in the analytical model by Ashby *et al.* 2000). Relationships for the elastic and plastic (plateau) behavior of low-density foams are given in Gibson and Ashby (1997). However, the elastic-plastic transition zone is extremely important for the deformation

behavior of composite structures. Therefore, the plane strain test is proposed in this paper to investigate the elastic-plastic transition zone.

The experimental determination of material properties of cellular materials is quite complicated since classical extensometers or strain gages are difficult to attach on the cellular surface which is extremely rough and structured. Young's modulus and the flow curve can be determined based on classical uniaxial tensile or compression tests (Papka and Kyriakides 1994, 1998, Gong *et al.* 2005). However, the determination of a second elastic constant, e.g., Poisson's ratio, is extremely difficult because the measurement of the transversal strains with classical methods is not possible. It is quite difficult to attach extensometers or strain gages on the cellular surface which is rough and extremely structured (cf. Fig. 1).

The experimental investigation of cellular solids has been studied in numerous research projects and different approaches to obtain complex stress states are reported in the scientific literature. However, an experimental specimen needs to comprise a representative volume and therefore must consist of a minimum amount of unit cells to avoid any edge effects and to represent macroscopic values. Classical test methods such as thin-walled tubes (Lefebvre *et al.* 1983) or simple shear tests (Rauch 1998) are difficult to achieve with respect to the specimen size as the evaluation procedures of these test methods require thin specimens. A tube specimen of a cellular material with, for example, 10 or more cells over the tube thickness can no longer be considered as thin and the assumption that the shear stress is constant over the thickness no longer holds. One possible way to overcome this problem is the generation of multiaxial stress states by using complex apparatus. For example, an enhanced Arcan test for biaxial testing of cellular solids is presented in Mohr and Doyogo (2003). However, the enhanced Arcan test requires the manufacturing of tapered specimens to avoid the heterogeneity problem (Wierzbicki and Doyoyo 2003). A triaxial system for axisymmetric stress (Deshpande and Fleck 2000) and a special loading system for biaxial and hydrostatic tension are used in Deshpande and Fleck (2001) and allow for the determination of the initial yield surface of porous materials. A similar axisymmetric test in conjunction with biaxial compression-compression tests are applied in Gioux *et al.* (2000). Here, the yield surfaces are determined for different commercial metal foams and aluminium honeycomb. A disadvantage of the axisymmetric testing method is that the practical realization requires a shim around the porous material in order to apply a hydrostatic pressure on the specimen. The shim carries a part of the effective load and therefore alters the measured data (Gioux *et al.* 2000). In Öchsner *et al.* (2003), a plane strain state realized due to a biaxial testing machine is proposed and the experimental realization is described in Öchsner *et al.* (2005). However, the realization of the above mentioned methods is connected with complex and expensive experimental equipment and might be not available in standard test laboratories. Therefore, a method based on a uniaxial strain test which is easy to realize in a universal testing machine is proposed in the following. This test aims not only to determine a second elastic constant but also further parameters of the yield criterion. The method is demonstrated based on a regular model structure by numerical simulation.

2. Constitutive modelling of porous materials

2.1 Elastic behavior

Under the classical assumptions of isotropy, small strains and linear relationships between the

second-order tensor σ_{ij} and the strain tensor ε_{ij} , the elastic stress-strain relation is given by general Hooke's law

$$\varepsilon_{ij} = \frac{1 + \nu}{E} \left(\sigma_{ij} - \frac{\nu}{1 + \nu} \delta_{ij} \sigma_{kk} \right) = C_{ijkl}^{-1} \sigma_{kl} \quad (1)$$

where E is Young's modulus, C_{ijkl} the fourth-order stiffness moduli tensor and ν Poisson's ratio. In a uniaxial tension or compression test, the only non-zero component σ_{xx} causes axial strain ε_{xx} and transverse strains $\varepsilon_{yy} = \varepsilon_{zz}$. Thus, one can determine the elastic constants, i.e., Young's modulus and Poisson's ratio from Eq. (1).

2.2 Plastic behavior

The classical assumption from solid materials, i.e., that the plastic behavior is incompressible, does no longer hold in the case of cellular materials. The plastic behavior is pressure-sensitive due to the cellular structure even when the pure base material is independent of the hydrostatic pressure in the plastic range. Therefore, the yield condition F needs to incorporate the hydrostatic pressure:

$$F = F(J_1^0, J_2, q_{ij}) = 0 \quad (2)$$

where $J_1^0 = \sigma_{ii}$ (\sim hydrostatic stress) is the first invariant of the spherical stress tensor σ_{ij}^0 , $J_2 = \frac{1}{2} s_{ij} s_{ji}$

the second invariant of the deviatoric stress tensor s_{ij} and q_{ij} the tensor of hardening parameters which includes the variables for isotropic and kinematic hardening. In many cases, Eq. (2) can be expressed for pressure-sensitive materials in the following additive form

$$F = \underbrace{\alpha(\varepsilon_{eff}^p) f_1(J_1^0) + f_2(J_2')}_f + f_3(k_s(\varepsilon_{eff}^p)) = 0 \quad (3)$$

where the classical yield condition ($\sim J_2'$) for solid metals is additively supplemented with an expression which incorporates the hydrostatic stress ($\sim J_1^0$). In Eq. (3), f_i ($i = 1, 2, 3$) are arbitrary scalar functions, ε_{eff}^p is the equivalent plastic strain (Chen and Hahn 1988), k_s is the yield stress under pure shear load and the parameter α weights the influence of the hydrostatic stress. It should be mentioned here that the yield stress k_s can be obtained from torsion tests (pure shear) or be calculated from the uniaxial tensile yield stress but the determination of α requires the realization of multi-axial stress states. Known examples for the yield condition based on Eq. (3) are e.g., the classical von Mises (cf. Eq. (4)) or Drucker-Prager (cf. Eq. (5)) yield condition or the Mahrenholz condition (Mahrenholtz and Ismar 1979, 1981) (cf. Eq. (6)) which has been successfully applied in Öchsner *et al.* (2003) for the description of the elastic-plastic transition behavior of cellular metals.

$$F = \sqrt{J_2'} - k_s(\varepsilon_{eff}^p) = 0 \quad \text{Von Mises} \quad (4)$$

$$F = \alpha(\varepsilon_{eff}^p) J_1^0 + \sqrt{J_2'} - k_s(\varepsilon_{eff}^p) = 0 \quad \text{Drucker-Prager} \quad (5)$$

$$F = \alpha(\varepsilon_{eff}^p) (J_1^0)^2 + \sqrt{J_2'} - (k_s(\varepsilon_{eff}^p))^2 = 0 \quad \text{Mahrenholz} \quad (6)$$

2.3 Uniaxial strain test

Under the classical assumption of small strains, the total strain increment $d\varepsilon_{ij}$ is assumed to be the sum of the elastic strain increment $d\varepsilon_{ij}^e$ and the plastic strain increment $d\varepsilon_{ij}^p$

$$d\varepsilon_{ij} = d\varepsilon_{ij}^e + d\varepsilon_{ij}^p \quad (7)$$

where the elastic strain increment can be obtained from Hooke's law (1) and the plastic strain increment increment from the associated flow rule (Chen and Hahn 1988)

$$d\varepsilon_{ij}^p = d\lambda \frac{\partial F}{\partial \sigma_{ij}} \quad (8)$$

Application of the chain rule with respect to the stress vector σ_{ij} gives the derivative of the scalar yield criterion (3) as:

$$\frac{\partial F(J_1^o, J_2)}{\partial \sigma_{ij}} = \frac{\partial F}{\partial J_1^o} \cdot \frac{\partial J_1^o}{\partial \sigma_{ij}} + \frac{\partial F}{\partial J_2} \cdot \frac{\partial J_2}{\partial \sigma_{ij}} = \alpha \cdot \frac{\partial f_1}{\partial J_1^o} \cdot \delta_{ij} + \frac{\partial f_2}{\partial J_2} \cdot s_{ij} \quad (9)$$

If Hooke's law (1) is applied for the elastic component and the associated flow rule (8) for the plastic component, the complete stress-strain relationship for a material obeying a yield criterion of form (3) is expressed as

$$d\varepsilon_{ij} = d\lambda \cdot \left(\alpha \cdot \frac{\partial f_1}{J_1^o \cdot \delta_{ij} + \frac{\partial f_2}{\partial J_2} \cdot s_{ij}} \right) + \frac{1+\nu}{E} \left(d\sigma_{ij} - \frac{\nu}{1+\nu} \delta_{ij} d\sigma_{kk} \right) \quad (10)$$

For the uniaxial strain (no wall friction, principal directions are *I*, *II*, *III*, cf. Fig. 3), we have

$$\sigma_I < 0 \wedge \varepsilon_I \neq 0 \quad (11)$$

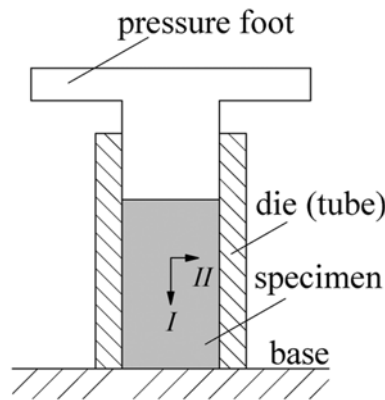


Fig. 3 Experimental realization of the uniaxial strain

$$\sigma_{II} \neq 0 \wedge \varepsilon_{II} = 0 \quad (12)$$

$$\sigma_{III} \neq 0 \wedge \varepsilon_{III} = 0 \quad (13)$$

where σ_i and ε_i can be directly measured during the experiment due to a load cell and an extensometer. Using Eqs. (11)-(13) with the associated flow rule (8) and Eq. (10), the increments of the plastic strains are given by:

$$d\varepsilon_i^p = d\lambda \left[\alpha \cdot \frac{\partial f_1}{\partial J_1^o} + \frac{\partial f_2}{\partial J_2} \cdot \frac{1}{3} (2\sigma_i - \sigma_{II} - \sigma_{III}) \right] \quad (14)$$

$$d\varepsilon_{II}^p = d\lambda \left[\alpha \cdot \frac{\partial f_1}{\partial J_1^o} + \frac{\partial f_2}{\partial J_2} \cdot \frac{1}{3} (-\sigma_i + 2\sigma_{II} - \sigma_{III}) \right] \quad (15)$$

Dividing Eq. (14) by (15) and rearranging, the parameter α is obtained as

$$\alpha = \frac{1}{3} \cdot \frac{\sigma_i \frac{\partial f_2}{\partial J_2} \left(1 + 2 \frac{d\varepsilon_{II}^p}{d\varepsilon_i^p} \right) - \sigma_{II} \frac{\partial f_2}{\partial J_2} \left(2 + \frac{d\varepsilon_{II}^p}{d\varepsilon_i^p} \right) + \sigma_{III} \frac{\partial f_2}{\partial J_2} \left(1 - \frac{d\varepsilon_{II}^p}{d\varepsilon_i^p} \right)}{\frac{\partial f_1}{\partial J_1^o} \left(1 - \frac{d\varepsilon_{II}^p}{d\varepsilon_i^p} \right)} \quad (16)$$

For small plastic strains (respectively at the beginning of the yielding), the quotient is $d\varepsilon_{II}^p/d\varepsilon_i^p \ll 1$ (respectively = 0) and the quantity α can be approximated by

$$\alpha \approx \frac{1}{3} \cdot \frac{\sigma_i \frac{\partial f_2}{\partial J_2} - 2\sigma_{II} \frac{\partial f_2}{\partial J_2} + \sigma_{III} \frac{\partial f_2}{\partial J_2}}{\frac{\partial f_1}{\partial J_1^o}} \quad (17)$$

The increments of plastic strain can be determined from Eq. (7) as

$$d\varepsilon_i^p = d\varepsilon_i - d\varepsilon_i^e = d\varepsilon_i - E \cdot d\sigma_i \quad (18)$$

$$d\varepsilon_{II}^p = \underbrace{d\varepsilon_{II}}_0 - d\varepsilon_{II}^e = -E \cdot d\sigma_{II} \quad (19)$$

$$d\varepsilon_{III}^p = \underbrace{d\varepsilon_{III}}_0 - d\varepsilon_{III}^e = -E \cdot d\sigma_{III} \quad (20)$$

while the elastic strain increments can be obtained from Hooke's law (1).

In the hardening theory of plasticity, the hardening parameter in the yield criterion can be related to the experimental uniaxial stress-strain curve. To this end, one needs to define a stress variable, called effective stress, which is a function of the stresses and some strain variables, called effective strain, which is a function of the plastic strains, so that they can be plotted and used to correlate the test results obtained by different loading conditions. Since the effective stress should reduce to the

stress σ_I in a uniaxial test, i.e., $\sigma_{eff} = \sigma_I$, it follows that the function f must be a constant c multiplied by the effective stress σ_{eff} to a power n (Chen and Hahn 1988)

$$f(\sigma_{ij}, \varepsilon_{eff}^p) = c \cdot (\sigma_{eff})^n \quad (21)$$

For the uniaxial test with $\sigma_{eff} = \sigma_I$; $\sigma_{II} = \sigma_{III} = 0$ and $J_1^o = \sigma_I$; $J_2 = \frac{1}{3}\sigma_I^2$, coefficient comparison, i.e.,

$$\alpha f_1(\sigma_I) + f_2(\sigma_I) = c \cdot \sigma_I^n \quad (22)$$

gives the parameters c and n . The effective plastic strain increment $d\varepsilon_{eff}^p$ can be defined in terms of the plastic work per unit volume in the form

$$dw^p = \sigma_{eff} d\varepsilon_{eff}^p = \sigma_{ij} d\varepsilon_{ij}^p = \sigma_I d\varepsilon_I^p + \sigma_{II} d\varepsilon_{II}^p + \sigma_{III} d\varepsilon_{III}^p \quad (23)$$

It follows from Eq. (23) using Eq. (1) and the results from Eq. (22) that in the case of the uniaxial strain the effective plastic strain increment is given by the following equation

$$d\varepsilon_{eff}^p = \frac{1}{\sigma_{eff}} \left[\sigma_I d\varepsilon_I^p - \sigma_{II} \frac{1}{E} (-\nu d\sigma_I + d\sigma_{II} - 2\nu d\sigma_{III}) - \sigma_{III} \frac{1}{E} (-\nu d\sigma_I - \nu d\sigma_{II} + d\sigma_{III}) \right] \quad (24)$$

Finally, it should be mentioned here that the elastic range is independent of the yield criterion and the following incremental relation can be directly derived based on Hooke's law as

$$\frac{d\sigma_I}{d\varepsilon_I} = K + \frac{4}{3}G \quad (25)$$

where $K + \frac{4}{3}G$ is known as the constrained modulus. The last equation may play an important role

for the experimental determination of the elastic material parameters of cellular materials. If Young's modulus E is obtained from an uniaxial tensile or compression test, then Poisson's ratio ν can be calculated from the slope $d\sigma_I/d\varepsilon_I$ in the elastic range of a uniaxial strain test. Using the well-known relationships between elastic constants (e.g., Chen and Hahn 1988), Eq. (25) can be rewritten as:

$$\frac{d\sigma_I}{d\varepsilon_I} = \frac{E}{3(1-2\nu)} + \frac{4}{3} \cdot \frac{E}{2(1+\nu)} \quad (26)$$

3. Finite element simulation

The FE simulation is performed with the commercial FE code MSC.Marc. Corresponding to the two different approaches, FE models for the unit cell and the homogenised structure are generated.

In the following, a *periodic* arrangement of cells (= infinite number) is considered where the influence of the free boundary can be disregarded. The FE model for the unit cell approach is shown in Fig. 4. The geometry corresponds to a cellular structure with the relative density $\rho_{rel} = \rho/\rho_{solid} = 0.7$. In order to reduce the number of unknowns and consequently the required computing

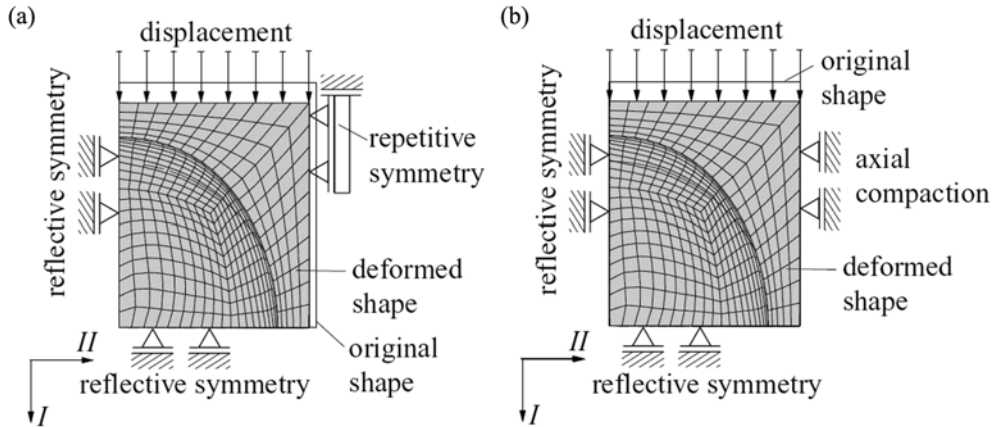


Fig. 4 FE model for the unit cell approach: (a) Uniaxial compression, (b) Uniaxial strain

time, only a typical *repeating* portion (unit cell) has been modelled. This simplification is applicable due to the symmetry of the geometry and the applied loads. Consequently, in order to simulate the behavior of the whole structure, i.e., *periodic*, certain symmetric boundary conditions must be introduced (Öchsner *et al.* 2003, Öchsner and Lamprecht 2003). Besides the reflective symmetric boundary conditions modelling the influence of the residual pore cell, repetitive symmetric boundary conditions are defined. They are imposing for the periodic case of adjacent cells the restriction that all nodes on a certain surface have the same displacement perpendicular to this surface. Two load cases can be distinguished: Fig. 4(a) shows the geometry with the boundary conditions according to a uniaxial compression test. In load case 4(b), the uniaxial strain is realized by inhibiting the deformation of the unit cell in the *II*- and *III*-direction. The material parameters of the structure's cell walls correspond to the aluminum alloy AlCuMg1. The plastic behavior of the

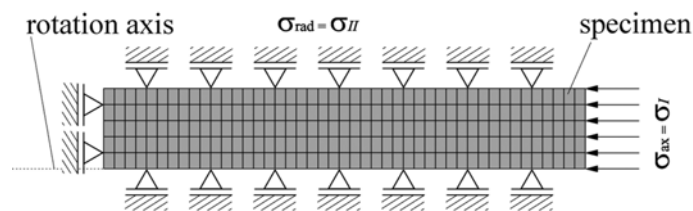


Fig. 5 Illustration of the idealized and homogenized FE model

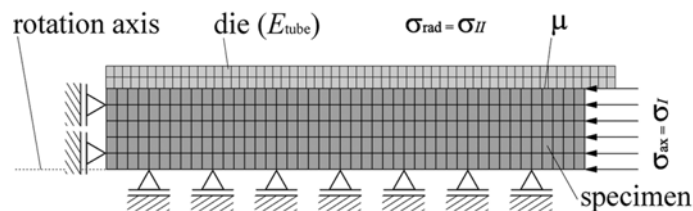


Fig. 6 Illustration of the homogenized FE model corresponding to the physical experiment

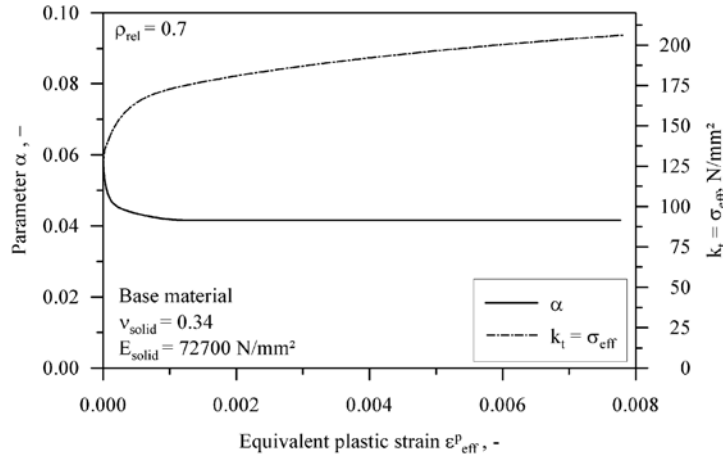


Fig. 7 Results from the unit cell approach

matrix material is described by the von Mises yield criterion (cf. Eq. (4)) and the corresponding associated flow rule. Furthermore, isotropic hardening is assumed for the matrix material where the equivalent plastic strain is taken as the isotropic hardening parameter (cf. Fig. 7, $\sigma_{eff} = \sigma_{eff}(\varepsilon_{eff}^p)$). The macroscopic stresses were obtained by summing up all the nodal reaction forces where a displacement boundary condition was prescribed and then dividing this value by the initial cross sectional area.

For the homogenized model of the uniaxial strain, axis-symmetric models are generated (cf. Figs. 5 and 6). The discretization of the specimen consists of axis-symmetric elements. The whole mesh of the specimen comprises in total 600 four node, iso-parametric elements with bilinear interpolation functions. To these elements, the effective material parameters obtained in the unit cell approach have been assigned. The load case shown in Fig. 5 is identical with the one defined for the uniaxial strain of the unit cell. In Fig. 6, the FE model has been extended by simulating the influence of the outer tube under the aspect of friction (μ) and finite stiffness of the tube material E_{tube} .

3.1 Unit cell approach

The results of the uniaxial compression test allow for the determination of different material parameters. According to Eq. (1), Young's modulus E and Poisson's ratio ν of the structure (not to be confused with the characteristic values of the base material denoted by index s 'solid': $E_s = 42780 \text{ N/mm}^2$, $\nu_s = 0.2784$) can be obtained.

Besides the uniaxial compression test, the load case of uniaxial strain is investigated. According to Eq. (16), the parameter α is evaluated for the Mahrenholz yield condition. Furthermore, the uniaxial tensile yield stress $k_t = \sigma_{eff}$ is determined. The results are shown in Fig. 7 in dependence of the equivalent plastic strain ε_{eff}^p .

The slope of the parameter α converges with increasing equivalent plastic strain to a constant value. Thus, the material remains in the investigated plastic range (cf. Fig. 2, region 2) compressible. The isotropic hardening of the structure is described by the constant increase of the tensile yield stress k_t . For the application of these material parameters in the numerical code, both curves have been approximated by polynomials $\alpha(\varepsilon_{eff}^p)$ and $k_t(\varepsilon_{eff}^p)$.

3.2 Homogenized material

In order to model larger parts of a cellular geometry, the structure has to be homogenized. The homogenization implies the assignment of the attributes of the cellular material to solid elements. The aim is to describe the response of bigger structures to non-symmetric loads without modelling the microstructure of each cell, which would fast exceed the resources of the available computer hardware. Instead of modelling the microstructure, the cellular structure is generated with few solid elements which exhibit the same properties and doing so, a much lower number of unknowns and therefore computing time is achieved. The definition, respectively allocation of the material attributes, in particular $\alpha(\varepsilon_{eff}^p)$ and $k_t(\varepsilon_{eff}^p)$ and implementation of the yield condition (6), is done with the Fortran User Subroutine UVSCPL of the MSC.Marc code. This routine allows very general material laws to be implemented, by updating e.g., the inelastic strain and the stress increment (Documentation 2003). Details of the implementation of the constitutive equation based on the fully implicit backward Euler scheme are given in Öchsner and Lamprecht (2003). Furthermore, Young's modulus E and Poisson's number ν , obtained from the uniaxial tension test, are defined.

First, the homogenized model is investigated with the boundary conditions illustrated in Fig. 5. These boundary conditions are equivalent to the uniaxial strain test of the unit cell approach. Therefore, identical results for the evaluated material parameters, e.g., ν , E , α , ... are obtained.

In Fig. 8, the correlation of the plasticity parameter α is exemplarily demonstrated. First, the slope of the input polynomial $\alpha(\varepsilon_{eff}^p)$, gained in the unit cell approach, as a function of the equivalent plastic strain ε_{eff}^p is drawn. In addition, α obtained by the postprocessing of the FE results of the homogenized model is visualized. Except for a minor deviation in the case of small ε_{eff}^p both slopes coincide. Consequently, it can be concluded that the homogenization is valid under the chosen parameters.

In the second step, the influence of certain phenomena occurring in the experimental realization is investigated (cf. Fig. 6). In the physical experiment, the constraining of the axial deformation is obtained by means of a tube. This tube is characterized by a finite stiffness E_{tube} which leads to a small deformation of the specimen in the radial direction. In the case of the idealized definition of

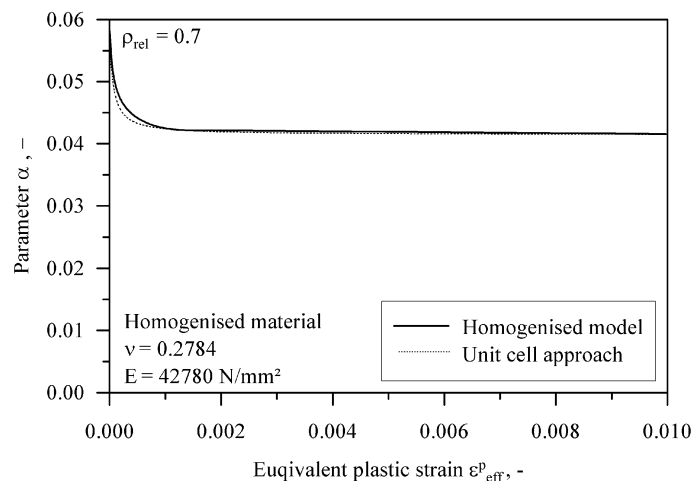


Fig. 8 Scope of α obtained by the uniaxial cell approach (Polyoma) and the homogenized model

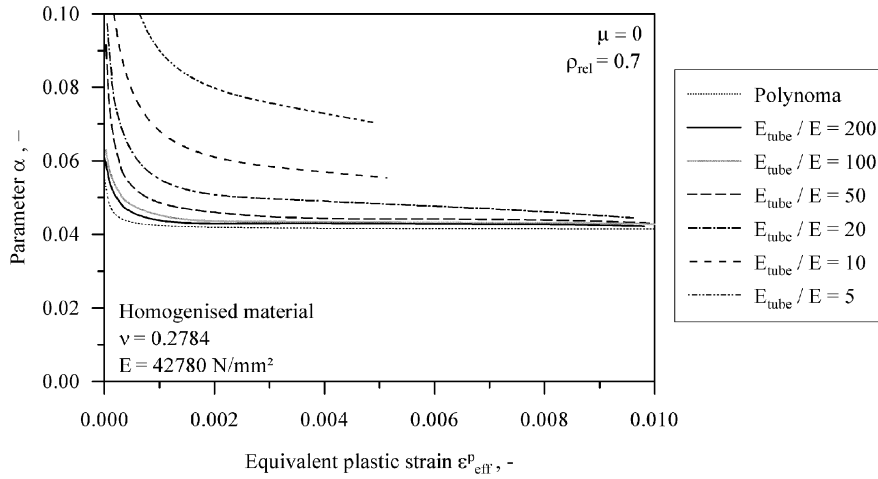


Fig. 9 Influence of the finite tube stiffness on the parameter α

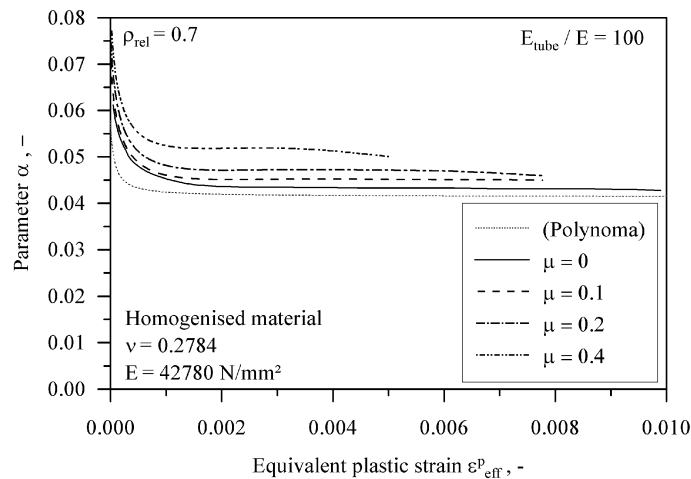


Fig. 10 Dependence of the parameter α on the friction coefficient μ

the boundary conditions according to Figs. 4 and 5, this deformation has been neglected. In the following, different ratios $E_r = E_{tube}/E$ are considered and the disturbance on the material parameter α is analyzed.

The results are illustrated in Fig. 9. As reference values, the input polynomial $\alpha(\epsilon_{eff}^p)$ is drawn by the dotted line. For high ratios E_r , good coincidence with the reference can be observed. However, the deviation to the polynomial significantly increases for small values of E_r , especially for low equivalent plastic strains. With increasing ϵ_{eff}^p , the divergence is decreasing and the slopes converge towards the exact solution.

Another important disturbance is the friction between the tube and the specimen. For the simple stick-slip model, only the friction coefficient μ is required to fully describe the tribological system. Four different values of μ are investigated for $E_r = 100$ (cf. Fig. 10).

Independent of the friction coefficient, all slopes of this stiffness ratio start in the same point.

With increasing equivalent plastic strain, the influence of the friction becomes visible. The increase of the parameter μ yields to higher convergence values for α .

4. Recommendations for experimental realization

In the following, the physical realization of the proposed experiment is elucidated and, based on the FE results, recommendations for the minimization of the disturbances are given.

As shown in Eq. (26), a second elastic value can be determined if e.g., Young's modulus E is already available. This possibility is especially interesting for cellular materials. Due to the condition of their surfaces, the attachment of measuring devices like strain gages or extensometers to determine the transverse strain in uniaxial compression test is difficult. Thus, ν normally cannot be calculated according to Eq. (1), like usually done with solid materials. The central aim of the experiment is to determine the material parameters α and k_l as a function of ε_{eff}^p . Therefore, according to formulae (16) and (24) the following values must be determined: $\sigma_l = \sigma_{ax}$, $\varepsilon_l = \varepsilon_{ax}$, $\sigma_{II} = \sigma_{III} = \sigma_r = \sigma_\theta$. The axial stress σ_{ax} can be obtained by measuring the force acting on the pressure foot, e.g. with the aid of a load cell, and dividing this value by the cross section area of the undeformed specimen. Also the axial displacement and therefore the axial strain ε_{ax} can be directly determined by means of an extensometer. However, the radial stress σ_r cannot be directly measured. Instead of this, the peripheral strain ε_θ on the outer surface of the tube might be obtained with the aid of a strain gage. Based on this value, analytic equations (e.g. Flügge 1962) for thick-walled cylinders under internal pressure (cf. Fig. 11) allow for the determination of the internal pressure p_i , which is identical to the radial stress of the specimen σ_r for $r = r_i$.

$$E \cdot \varepsilon_\theta = \sigma_\theta - \nu \cdot \sigma_r - \nu \cdot \sigma_{ax} \quad (27)$$

Hooke's law in polar coordinates is described in Eq. (27) for a thick walled cylinder. For the outer

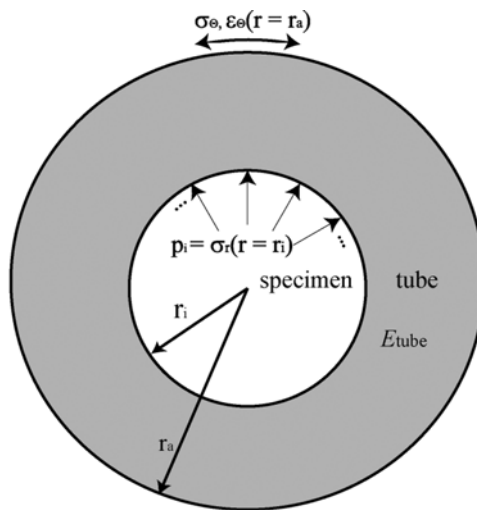


Fig. 11 Boundary conditions for the thick-walled cylinder

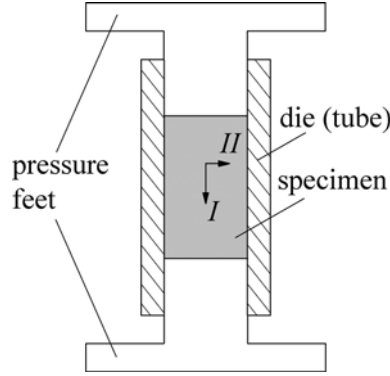


Fig. 12 Experimental realization of the double-sided uniaxial strain test

surface of the cylinder ($r = r_a$) the radial stress σ_r is zero. As an additional simplification, one can introduce that the axial stress σ_{ax} of the cylinder is identical zero which is perfectly fulfilled in the case of free ends of the tube and neglected friction. Thus the peripheral stress σ_θ can be approximately calculated with the measured value ε_θ and the known stiffness of the tube material E_{tube} .

$$\sigma_\theta = \frac{r_i^2 \cdot p_i}{r_a^2 - r_i^2} \left(1 + \frac{r_a^2}{r^2} \right) \quad (28)$$

Now, formula (28) enables the determination of the internal pressure $p_i = \sigma_r = \sigma_{II}$. Thus, all required values are available.

To obtain accurate results, the influence of the disturbing friction and finite stiffness of the tube material must be minimized. The friction can be significantly reduced by adding a lubricate to the tribological system created by the surfaces of specimen and tube. In Chengfeng *et al.* (2001), the application of room-temperature ionic liquids is investigated. For the contact of steel and aluminium, the lubricate L106 reduces the high friction coefficient (dry St/Al $\mu \approx 0.45$) by one order of magnitude to $\mu = 0.040$. With respect to the surface of the porous material (reservoirs for the lubricate, hydrodynamic flanks, etc.) even lower values for the friction coefficient can be expected. Another possible strategy to decrease the negative effect of friction is to reduce the inhomogeneity of the deformation of the specimen by compacting it from two sides as visualized in Fig. 12.

The second major influence is the finite stiffness of the tube material. As shown in section 3.2, this influence can be minimized by investigating only specimens with relatively low Young's modulae. If the stiffness ratio is high, e.g., $E_r > 100$, the observed deviation is small. This assumption holds normally for commercial metal foams (e.g., ALPORAS, Cymat, ERG) with $\rho/\rho_{solid} \leq 0.2$, (Ashby *et al.* 2000). However, as for the tube material typically steel will be employed, this requirement limits Young's modulus of the specimen to values below 2100 N/mm². Another possibility is the increase of the outer diameter of the steel tube. The higher structural stiffness of the tube leads to better results for rising ratios $r_{tube}/r_{specimen}$ (cf. Fig. 13).

In order to estimate the influence of the disturbance as well as to have a possibility for the correction of the results, the starting value for $\alpha(\varepsilon_{eff}^p = 0) = \alpha_0$ can be determined only in

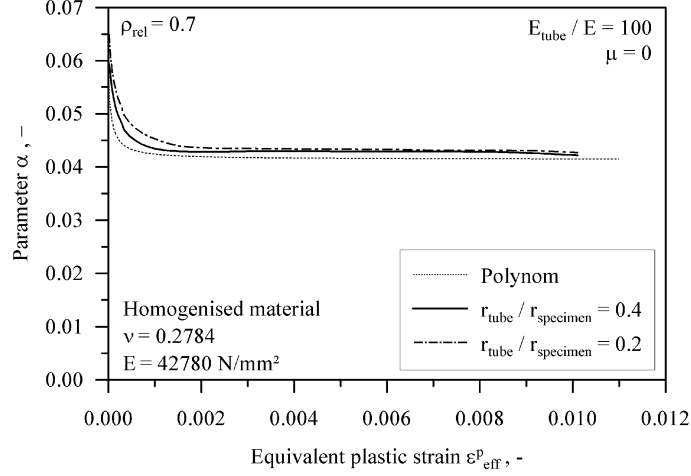


Fig. 13 Influence of the relative tube thickness on the parameter α

dependence of Poisson's ratio ν . Starting with Eq. (27) and $\sigma_r = \sigma_\theta$, the ratio $\sigma_z/\sigma_r = \sigma_z/\sigma_\theta$ can be expressed as

$$\frac{\sigma_z}{\sigma_r} = \frac{\sigma_z}{\sigma_\theta} = \frac{1 - \nu}{\nu} \quad (29)$$

At the beginning of the plastification ($d\varepsilon_i^p = 0$), Eq. (16) with ratio (29) yields in the case of Mahrenholz yield condition (6) after some transformations to

$$\alpha_0(\nu) = \frac{1}{6} \cdot \frac{1 - 2\nu}{1 + \nu} \quad (30)$$

Consequently $\alpha_0(\nu = 0.2784) = 0.05778$ can be calculated based on the elastic properties. This result coincides with the value of the polynomial $\alpha(\varepsilon_{eff}^p = 0)$ obtained in section 3.1 for the ideal case (infinite stiffness of the tube material, no friction).

5. Conclusions

In the scope of this article, the uniaxial strain test is suggested as an experimental setup for the determination of material parameters of porous materials. In addition to the possibility of obtaining a second elastic constant next to e.g., Young's modulus E , the plastic behavior of the specimen can be determined for miscellaneous yield conditions. This is successfully demonstrated for the case of Mahrenholz yield condition by means of FE analyses. Therefore, this easily realizable experiment might be an alternative for more complex experiments that require different multi-axial stress states. Furthermore, the influence of the finite stiffness of the die and the wall friction on the determination of the plasticity parameter α in Mahrenholz yield condition is investigated. Based on these results, recommendations for the optimization of the experimental setup are given. The experimental realization of the uniaxial strain is reserved for our future research work.

Acknowledgements

T. Fiedler and A. Öchsner are grateful to Portuguese Foundation of Science and Technology (FCT) for financial support.

References

- Ashby, M.F., Evans, A., Fleck, N.A., Gibson, L.J., Hutchinson, J.W. and Wadley, H.N.G. (2000), *Metal Foams: A Design Guide*, Butterworth-Heinemann, Boston.
- Balch, D.K. and Dunand, D.C. (2002), *Processing and Properties of Lightweight Cellular Metals and Structures*, TMS, Warrendale.
- Chen, W.F. and Hahn, D.J. (1988), *Plasticity for Structural Engineers*, Springer Verlag, New York.
- Chengfeng, Y., Weimin, L., Yunxia, C. and Laigui, Y. (2001), "Room-temperature ionic liquids: A novel versatile lubricant", *Chem. Commun.*, **21**, 2244-2245.
- Deshpande, V.S. and Fleck, N.A. (2000), "Isotropic constitutive models for metallic foams", *J. Mech. Phys. Solids*, **48**, 1253-1283.
- Deshpande, V.S. and Fleck, N.A. (2001), "Multi-axial yield behaviour of polymer foams", *Acta Mater.*, **49**, 1859-1866.
- Documentation (2003), *MSC.Marc Volume D*, MSC Software Corporation.
- Flügge, W. (1962), *Handbook of Engineering Mechanics*, McGraw-Hill Book Company, New York.
- Gibson, L.J. and Ashby, M.F. (1997), *Cellular Solids*, Cambridge University Press, Cambridge.
- Gioux, G., McCormack, T.M. and Gibson, L.J. (2000), "Failure of aluminium foams under multiaxial loads", *Int. J. of Mech. Sci.*, **42**, 1097-1117.
- Gong, L. and Kyriakides, S. (2005), "Compressive response of open-cell foams. Part II : Initiation and evolution of crushing", *Int. J. Solids Struct.*, **42**, 1381-1399.
- Gong, L., Kyriakides, S. and Jang, W.Y. (2005), "Compressive response of open-cell foams. Part I : Morphology and elastic properties", *Int. J. Solids Struct.*, **42**, 1355-1379.
- Hartmann, M., Reindel, K. and Singer, R.F. (1998), "Microstructure and mechanical properties of cellular magnesium matrix composites", *Mater. Res. Soc. Symp. Proc.*, **521**, 211-216.
- Kiser, M., He, M.Y. and Zok, F.W. (1999), "The mechanical response of ceramic microballoon reinforced aluminum matrix composites under compressive loading", *Acta Mater.*, **47**, 2685-2694.
- Körner, C. and Singer, R.F. (2000), "Processing of metal foams - Challenges and opportunities", *Adv. Eng. Mater.*, **2**, 159-165.
- Lefebvre, D., Chebl, C., Thibodeau, L. and Khazzarie, E. (1983), "A high-strain biaxial-testing rig for thin-walled tubes under axial load and pressure", *Exp. Mech.*, **23**, 384-392.
- Mahrenholtz, O. and Ismar, H. (1979), "Ein Modell des elastisch-plastischen Übergangsverhaltens metallischer Werkstoffe", *Abh. Braunschweig Wiss. Gesell.*, **30**, 138-144.
- Mahrenholtz, O. and Ismar, H. (1981), "Zum elastisch-plastischen Übergangsverhalten metallischer Werkstoffe", *Ing-Archiv*, **50**, 217-224.
- Mohr, D. and Doyogo, M. (2003), "A new method for the biaxial testing of cellular solids", *Exp. Mech.*, **43**, 173-182.
- Öchsner, A. and Lamprecht, K. (2003), "On the uniaxial compression behavior of regular shaped cellular solids", *Mech. Res. Commun.*, **30**, 573-579.
- Öchsner, A., Winter, W. and Kuhn, G. (2003a), "On an elastic-plastic transition zone in cellular metals", *Arch. Appl. Mech.*, **73**, 261-269.
- Öchsner, A., Winter, W. and Kuhn, G. (2003b), "FE-Simulation of the elastic-plastic transition zone of cellular metals under complex loading conditions", *Proc. of the 15th Int. Conf. of Computer Methods in Mechanics CMM-2003*, Poland, June.
- Öchsner, A., Kuhn, G. and Grácio, J. (2005), "Investigation of cellular solids under biaxial stress states", *Exp. Mech.*, **45**, 325-330.

- Papka, S.D. and Kyriakides, S. (1994), "In-plane compressive response and crushing of honeycomb", *J. Mech. Phys. Solids*, **42**, 1499-1532.
- Papka, S.D. and Kyriakides, S. (1998), "In-plane crushing of a polycarbonate honeycomb", *Int. J. Solids Struct.*, **35**, 239-267.
- Rauch, E.F. (1998), "Plastic anisotropy of sheet metals determined by simple shear tests", *Mat. Sci. Eng. A*, **241**, 179-183.
- Wierzbicki, T. and Doyoyo, M. (2003), "Determination of the local stress-strain response of foams", *J. Appl. Mech.*, in press.